Article:
Kulmaczewski, R and Halcrow, MA orcid.org/0000-0001-7491-9034 (2016) Structures and Spin States of Crystalline [Fe(NCS)2L2] and [FeL3]2+ Complexes (L = an Annelated 1,10-Phenanthroline Derivative). CrystEngComm, 18 (14). pp. 2570-2578.

https://doi.org/10.1039/C6CE00163G

Structures and Spin States of Crystalline $[Fe(NCS)_2L_2]$ and $[FeL_3]^{2+}$ Complexes (L = an Annelated 1,10-Phenanthroline Derivative)†

Rafal Kulmaczewski and Malcolm A. Halcrow*

The phase behaviour and spin states of $[Fe(NCS)_2(dpq)_2]$ (**1**; dpq = dipyrido[3,2-*f*:2′,3′-*h*]quinoxaline), $[Fe(NCS)_2(dppz)_2]$ (**2**; dppz = dipyrido[3,2-*a*:2′3′-*c*]phenazine) and $[Fe(NCS)_2(dppn)_2]$ (**3**; dppn = dipyrido[3,2-*a*:2′3′-*c*]benzophenazine) have been investigated. Solvent-free **1** and **2** are isostructural and low-spin in the crystalline state, in contrast to previously published **2**·py (py = pyridine) which exhibits a hysteretic spin-crossover (SCO) transition near 140 K. The inactivity of **1** and **2** towards SCO may relate to their more crowded intermolecular lattice environment, particularly two very short intermolecular anion…π contacts involving the NCS^- ligands. Two solvate phases of **1** are also described, including **1**·2py which undergoes gradual SCO with $T_{½}$ *ca.* 188 K. Bulk samples of **2** and **3** are predominantly low-spin and isostructural with the crystals of **2** by powder diffraction, but bulk samples of **1** contain an extra phase that exhibits hysteretic SCO, but was not crystallographically characterised. Crystal structures of low-spin $[Fe(dppz)_3][ClO_4]_2$ (**4**) and a solvate of $[Fe(dppn)_3][BF_4]_2$ (**5**) are also described, and are the first homoleptic complexes of these ligands to be crystallographically characterised.

Introduction

Spin-crossover (SCO) complexes exhibit a reversible high ⇌ low spin-state rearrangement under a stimulus of temperature or pressure.[1-3] A spin-transition causes measurable changes to the physical properties of a molecular solid, including its colour,[4] magnetic moment,[4] conductivity,[5] dielectric constant[6] and particle size and shape.[7] Moreover, in addition to their own intrinsic functionality, spin-transition molecules can be auxiliary switching centers[8] in multifunctional fluorescent,[9] semiconducting[10] and magnetic materials.[11] The spin-transition phenomenon also functions in soft materials[12] and at the nanoscale,[13] and the relationship between particle size and switching functionality is now quite well understood.[14] Thanks to this wide applicability, SCO complexes are one of the most widely studied types of functional molecule-based material.[1-3]

Many of the above applications require materials that undergo SCO abruptly, near room temperature and with thermal hysteresis. Few compounds exhibit this combination of switching properties, and the crystal engineering of molecular solids with bespoke SCO characteristics is still a challenge.[15] We have proposed that cooperative (abrupt and hysteretic) SCO switching can be favoured in materials containing complexes of aromatic ligands, that interdigitate in the crystal through π-π contacts. This gives a large contact surface area between nearest neighbour molecules, thus increasing mechanical coupling between them. The structural changes accompanying SCO should be propagated through a crystal lattice more effectively in such cases, leading to increased cooperativity.[15]

One system that supports that suggestion is *cis*-$[Fe(NCS)_2L_2]$ [L = 2,2′-bithiazoline (btz), 2,2′-bipyridine (bipy), 1,10-phenanthroline (phen) and dipyrido[3,2-*a*:2′3′-*c*]phenazine (dppz); Scheme 1]. These compounds follow a consistent trend in their SCO cooperativity (py = pyridine):[16]

$[Fe(NCS)_2(btz)_2]$ (gradual)[17]
< $[Fe(NCS)_2(bipy)_2]$ (abrupt)[18]
≈ $[Fe(NCS)_2(phen)_2]$ (abrupt)[19]
< $[Fe(NCS)_2(dppz)_2]$·py (abrupt, wide hysteresis)[20]

The compounds all adopt packing motifs based on molecular networks of interdigitating L ligands. The trend in cooperativity was attributed to the stronger π-π overlap between the molecules, with increased aromaticity and annelation of the L ligands. More recent studies of $[Fe(NCS)_2(dppz)_2]$·py confirmed that view, showing that the dihedral angle between the least squares planes of the dppz ligands (Ψ) contracts by 15° during SCO.[21-23] Cooperative motion of the ligands about the metal ions during the transition is mediated by the stacks of dppz ligands in the crystal, leading to SCO hysteresis which can be as wide as 60 K in this compound. Many other complexes of the *cis*-$[Fe(NCS)_2L_2]$ type also exhibit SCO, but adopt different forms of crystal packing and are not considered to be part of this structure:function correlation.[24-29]

School of Chemistry, University of Leeds, Leeds, UK LS2 9JT. Fax: (+44) 113 343 6565. E-mail: m.a.halcrow@leeds.ac.uk

†Electronic Supplementary Information (ESI) available: additional crystallographic Figures and Tables; and, synthetic and characterisation data for bulk samples of the complexes, including X-ray powder diffraction and magnetic susceptibility measurements. CCDC-1430803-1430811 and 1456588-1456590. See

DOI: 10.1039/x0xx00000x

As part of our efforts to develop our ideas about molecular interdigitation and SCO,[30,31] we report a new investigation of the $[Fe(NCS)_2L_2]$ system using the annelated bipyridyl *L* ligands dppz, dipyrido[3,2-*f*:2′,3′-*h*]quinoxaline (dpq) and dipyrido[3,2-*a*:2′,3′-*c*]benzo[*i*]phenazine (dppn; Scheme 1). Our aims were to extend the structure:function relationship described in the previous paragraph, and to obtain the solvent-free phase of $[Fe(NCS)_2(dppz)_2]$ for comparison with its pyridine solvate.[20,21] We also report crystal structures of salts of $[Fe(dppz)_3]^{2+}$ and $[Fe(dppn)_3]^{2+}$, which were obtained during the course of this work. Although dppz in particular is widely used in photoactive metal complexes,[32] these are the first homoleptic complexes of dppz and dppn to be structurally characterised.

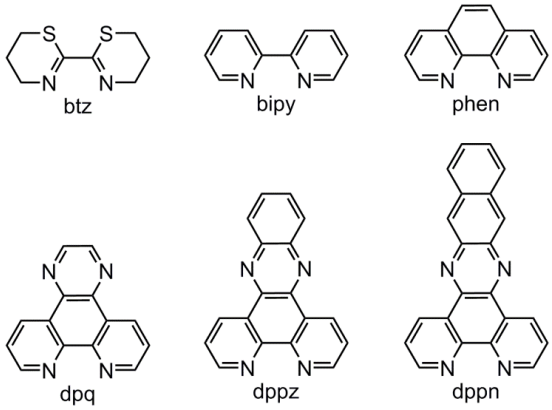

Scheme 1 Ligands referred to in this work.

Results and Discussion

The synthesis of $[Fe(NCS)_2L_2]$ (*L* = dpq, **1**;[33] *L* = dppz, **2**;[20-23] *L* = dppn, **3**) was pursued by several procedures based on literature protocols,[17-20,23,26,27] involving the *in situ* generation of $Fe[NCS]_2$ and its subsequent treatment with *L*. In each case a mixture of materials was obtained with differing degrees of crystallinity which included **1**-**3**; salts of the corresponding $[FeL_3]^{2+}$ complexes; $[Fe(NCS)_2(py)_2L]$ (where pyridine (py) was present in the reaction mixture);[34] and/or free *L* ligand.[30] The complexity of the product mixtures may reflect the lower solubility of the dpq, dppz and dppn ligands and their complexes, compared to the simpler heterocyclic chelates that are usually used for this type of chemistry.[24-29] Single crystals of the desired compounds were isolated from the reaction mixtures by Pasteur separation, for structural analysis.

Solvent-free crystals of **1** and **2** are isomorphous in the space group *C*2/*c*, their asymmetric unit containing half a complex molecule with Fe(1) spanning a C_2 symmetry axis (Fig. 1, Table 1). The Fe–N distances in both crystals are almost invariant at room and low temperatures, and show the complexes are low-spin in this crystal phase. That was confirmed by the volume of the FeN_6 coordination octahedron (V_{Oh}), which is 9.8-9.9 Å^3 in each structure (Table 1). Other compounds of the $[Fe(NCS)_2L_2]$ type reliably exhibit $V_{Oh} \approx 10$ Å^3 in their low-spin state, and 13 Å^3 when high-spin.[25] The angular distortion indices Σ and Θ, which are also used to monitor

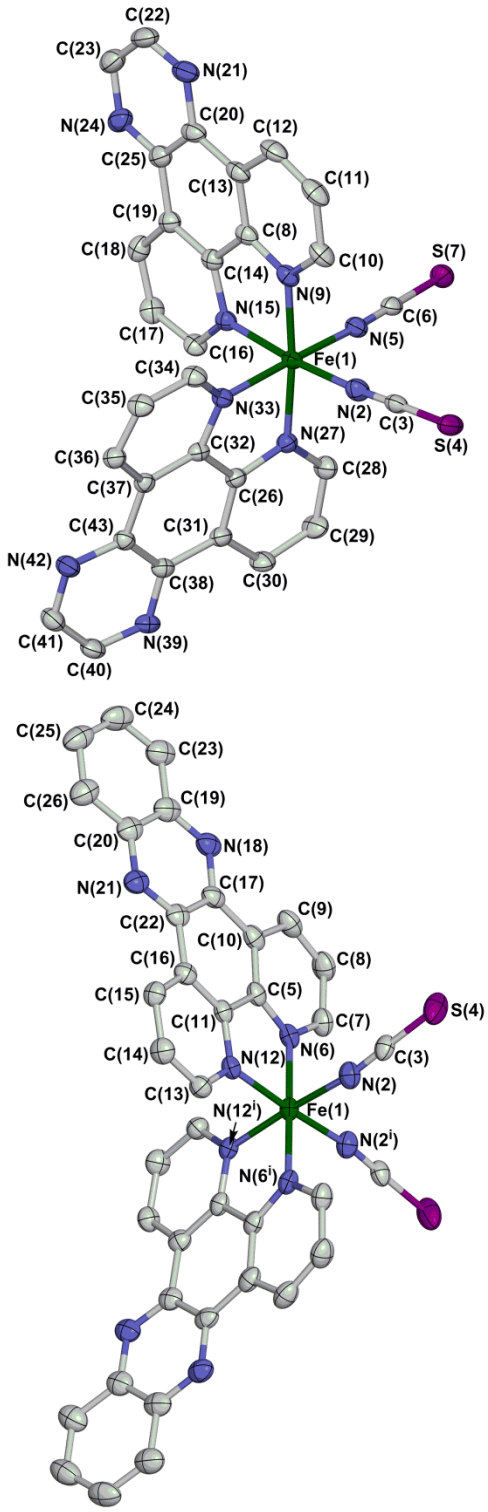

Fig. 1 Views of the complex molecules in the low temperature structures of **1**·2py (top) and **2** (bottom), showing the atom numbering schemes (the same atom numbering is also used for the other structures in this work). Displacement ellipsoids are at the 50 % probability level, and H atoms have been omitted for clarity. Symmetry code: (i) –*x*, *y*, $^3/_2$–*z*. Colour code: C, white; Fe, green; N, blue; S, purple.

crystallographic metal ion spin-states,[15] are less clear-cut for this type of compound and do not show a clear boundary between high-spin and low-spin structures.[25,37] The only

Table 1 Selected bond lengths and angles (Å, °) for solvent-free $[Fe(NCS)_2(dpq)_2]$ (**1**) and $[Fe(NCS)_2(dppz)_2]$ (**2**). See Fig. 1 for the atom numbering scheme. V_{Oh} is the volume of the octahedron defined by the FeN_6 coordination sphere (Å^3); Σ and Θ are bond angle parameters characteristic for the spin state of the complex;[25,35-37] and Ψ is the dihedral angle between the least squares planes of the dpq or dppz ligands in the molecule (ESI†).[22]

	1		**2**	
T [K]	120	290	120	290
Fe(1)–N(2)	1.934(2)	1.931(3)	1.938(3)	1.937(3)
Fe(1)–N(6)	1.964(2)	1.979(3)	1.968(3)	1.962(3)
Fe(1)–N(12)	1.958(2)	1.969(3)	1.966(3)	1.972(3)
Fe(1)–N(2)–C(3)	165.6(7)/ 178.0(11)[a]	167.8(9)/ 175.9(13)[a]	169.2(3)	167.9(6)/ 174.9(9)[a]
N(2)–C(3)–S(4)	178.7(11)/ 177.3(16)[a]	175.1(13)/ 172(2)[a]	178.1(3)	177.2(8)/ 173.3(14)[a]
V_{Oh}	9.833(9)	9.941(10)	9.904(10)	9.894(11)
Σ	43.1(4)	43.1(4)	45.4(4)	46.6(5)
Θ	76	82	78	81
Ψ	86.24(3)	86.08(4)	87.31(2)	88.34(3)

[a]The unique NCS^- ligand is disordered over two sites.

significant difference between the compounds at different temperatures is in the unique NCS^- ligand, which is crystallographically ordered in the low temperature structure of **2** but disordered over two sites in the other refinements (Table 1). That may reflect the close intermolecular contacts involving that group which are described below.[38]

The low-spin nature of solvent-free **1** and **2** was unexpected, since solvated phases of both complexes are SCO-active.[20-23,33] Moreover, only one other compound of the *cis*-$[Fe(NCS)_2L_2]$ type is known to be low-spin at room temperature.[24,39] Insight into this question is provided by the intermolecular interactions in the materials. The crystal packing in **1** and **2** is comprised of zig-zag chains of stacked of dpq and dppz ligands parallel to [001] (Fig. 2), which are linked into three dimensions by a very short anion…π interaction[40] between S(4) and the dpq or dppz ligand related by ½+*x*, –½+*y*, *z* (***a*** in Fig. 3). This has an S…centroid distance of 3.04-3.14 Å, which is 0.4-0.5 Å shorter than the sum of the van der Waals radii of an S atom (1.85 Å) and an arene (1.7 Å). In contrast, SCO-active **2**·py has a more extended two-dimensional array of intermolecular π-stacking, but these molecular sheets are well separated from each other by the pyridine solvent (Fig. 2). Thus, the lattice environment around the iron center is much more crowded in the solvent free crystals than in **2**·py (ESI†). As well as the anion…π interaction, the NCS^- ligands in **1** and **2** experience two C–H…S (***b*** and ***c*** in Fig. 3) and one C–H…C (***d***) intermolecular contacts to the NCS^- ligand, and one short π-π interaction between overlapping dpq or dppz ligands (***e***). This intermolecular steric crowding, most notably the anion…π interaction, probably inhibits the structural rearrangement that would accompany SCO in solvent-free **1** and **2**.

Two crystalline solvated phases of **1** were also obtained. First is **1**·$2C_2H_4Cl_2$ which, in contrast to the solvent-free complex, is fully high-spin at 100 K (Table 2). Notably, the

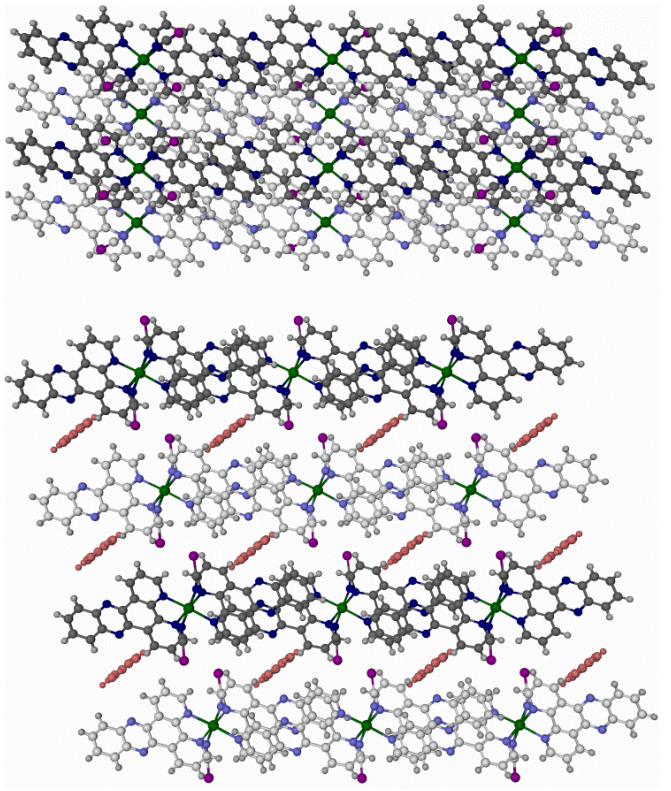

Figure 2 Comparison of the crystal packing of low-spin **2** (top) and SCO-active **2**·py (bottom).[22] Both views are along the crystallographic [010] vector, and alternate 1D chains (**2**) or 2D layers (**2**·py) of π-stacked molecules have pale and dark coloration. Colour code: C, white or dark gray; H, pale gray; Fe, green; N, pale or dark blue; S, purple; pyridine solvent, red.

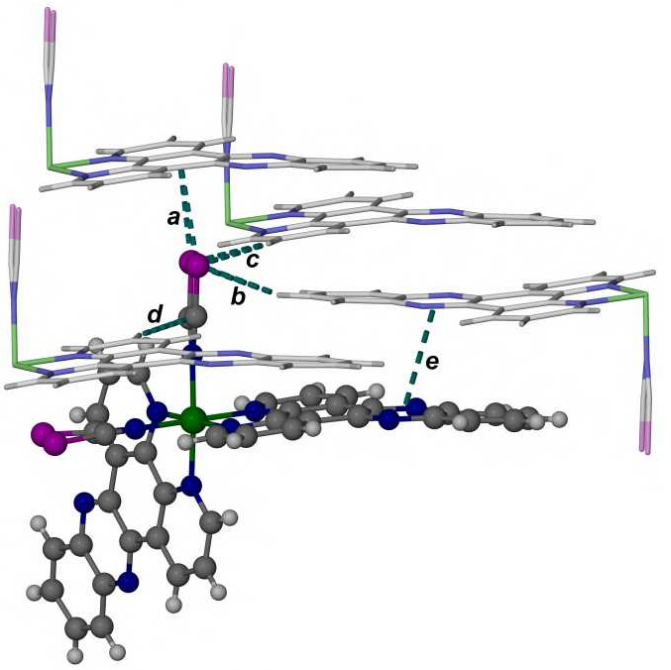

Figure 3 View highlighting the unique short intermolecular contacts in **2** at 290 K. Both disorder sites of the NCS^- ligands are shown, but the symmetry-related interactions to the other NCS^- and dpq ligands in the C_2-symmetric molecule are not included for clarity. Colour code: C, white or dark gray; H, pale gray; Fe, pale or dark green; N, pale or dark blue; S, pale or dark purple.

coordination sphere of this complex is significantly more distorted than the other compounds in this work, as evidenced by a much larger trigonal distortion parameter Θ[35] and a particularly small inter-ligand angle Ψ.[22] Molecules of **1** in this pseudopolymorph associate through π-stacking into 1D chains parellel to [111], which are in turn linked into sheets by intermolecular C–H...S contacts. The sheets of complex molecules are separated by well-defined layers of 1,2-dichloroethane solvent (ESI†).

The second solvate of **1** is **1**·2py, which was of interest for comparison with SCO-active **2**·py.[20-23] Recrystallisation of **1** from pyridine/diethyl ether afforded a mixture of **1**·2py (plates) and [Fe(NCS)$_2$(py)$_2$(dpq)]·py (twinned needles; ESI†).[34,41] Structure refinements at five temperatures demonstrated a gradual thermal SCO in **1**·2py between 290 K and 120 K, when it is fully high-spin and low-spin respectively (Fig. 4 and Table 2). The SCO midpoint temperature ($T_{½}$) is 188±2 K, based on the evolution of the complex's metric parameters upon cooling. The gradual transition profile in Fig. 4 is mirrored in the temperature dependence of the unit cell parameters which exhibit small discontinuities near 240 and 160 K, the approximate onset and end-points of the spin transition (ESI†). The gradual SCO in **1**·2py contrasts with the highly cooperative spin transition shown by **2**·py.[20-23]

The molecular structure in high-spin **1**·2py is less distorted than in **1**·2C$_2$H$_4$Cl$_2$, which may account for its activity towards SCO. In particular the inter-ligand angle (Ψ) is closer to the ideal value of 90°, and is almost the same in both spin states. Hence the change in Ψ between the spin states, which is responsible for the SCO hysteresis in **2**·py,[22] does not take place in **1**·2py. The complex molecules in **1**·2py also associate into 1D chains through intermolecular π...π interactions, this time parallel to the $\{\bar{1}10\}$ crystal vectors. In contrast to **1**·2C$_2$H$_4$Cl$_2$, however, there are no intermolecular contacts between the chains in **1**·2py, which are separated by the solvent molecules (ESI†).

Bulk samples of **1**-**3** prepared in this study all contained between 0.5-2.5 equiv lattice water by microanalysis, and were rarely phase-pure by powder diffraction (ESI†). The behaviour of **2** and **3** was quite consistent between the samples, which each contained solvent-free **2** (or the equivalent isostructural phase of **3**) as the major component. They were also fully, or predominantly, low-spin between 3-300 K from magnetic susceptibility and IR data (ESI†), although in some cases a small upturn in $\chi_M T$ above 250 K indicated the onset of gradual SCO centred above room temperature.[38] Samples of **1** were more variable, and contained differing amounts of a hysteretic SCO-active phase ($T_{½}$ = 154 K, $\Delta T_{½}$ = 6 K) as well as the predominantly low-spin sovent-free material (ESI†). X-ray powder diffraction of a sample containing *ca.* 80

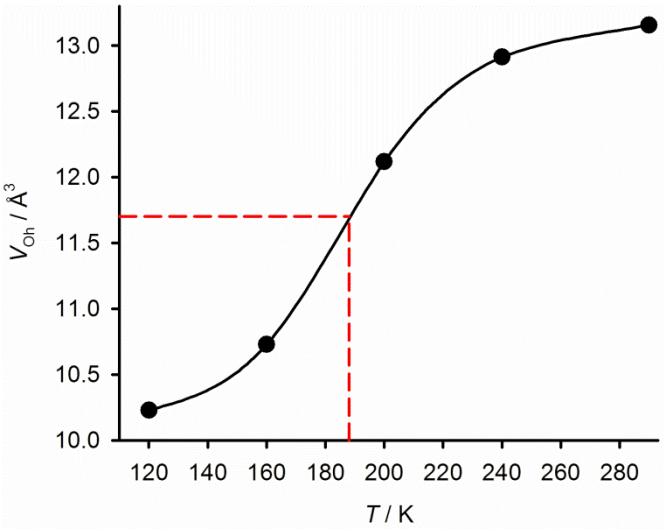

Figure 4 The spin-crossover transition in **1**·2py, as measured from the volume of the octahedron defined by the FeN$_6$ coordination sphere (V_{Oh}, Table 2). The dashed lines show the estimated midpoint of the transition at $T_{½}$ = 188 K.

Table 2 Selected bond lengths and angles (Å, °) for the solvated forms of [Fe(NCS)$_2$(dpq)$_2$] (**1**). See Fig. 1 for the atom numbering scheme. Other details as for Table 1.

	1·2C$_2$H$_4$Cl$_2$	**1**·2py				
T [K]	100	120	160	200	240	290
Fe(1)–N(2)	2.060(2)	1.9478(19)	1.961(3)	2.047(3)	2.075(4)	2.080(3)
Fe(1)–N(5)	2.091(2)	1.9656(18)	1.983(3)	2.047(3)	2.079(3)	2.093(2)
Fe(1)–N(9)	2.205(2)	1.9896(18)	2.029(3)	2.112(3)	2.173(3)	2.185(2)
Fe(1)–N(15)	2.226(2)	1.9897(17)	2.037(3)	2.143(2)	2.206(3)	2.221(2)
Fe(1)–N(27)	2.212(2)	1.9796(17)	2.017(3)	2.107(2)	2.161(3)	2.177(2)
Fe(1)–N(33)	2.234(2)	1.9932(17)	2.040(2)	2.146(2)	2.208(3)	2.235(2)
Fe(1)–N(2)–C(3)	173.5(2)	175.49(17)	177.0(3)	179.7(3)	178.6(3)	177.7(3)
Fe(1)–N(5)–C(6)	174.4(2)	176.52(17)	176.4(3)	175.2(3)	174.6(3)	174.1(2)
N(2)–C(3)–S(4)	178.4(3)	178.55(19)	179.1(3)	178.9(3)	178.7(4)	178.9(3)
N(5)–C(6)–S(7)	178.2(3)	179.6(2)	179.5(3)	179.8(3)	179.1(4)	179.3(3)
V_{Oh}	13.048(9)	10.230(6)	10.728(9)	12.118(10)	12.912(12)	13.157(9)
Σ	81.9(3)	40.0(2)	47.8(4)	63.6(3)	73.0(4)	76.1(3)
Θ	251	86	102	141	162	170
Ψ	73.66(3)	79.79(2)	79.40(2)	79.19(2)	78.80(3)	78.41(2)

% of this SCO-active phase showed it is not isostructural with any phase of **1** we have crystallographically characterised, or with the related SCO-active complex $[Fe(NCS)_2(phen)_2]$.[19] It may, however, correspond to the hydrated phase of **1** that has been previously reported by others.[33]

Single crystals of $[Fe(dppz)_3][ClO_4]_2$ (**4**) and $[Fe(dppn)_3][BF_4]_2{\cdot}3MeOH{\cdot}H_2O$ (**5**·3MeOH·H_2O) were also obtained during the course of this work. Few crystal structures of homoleptic complexes of annelated 1,10-phenanthroline derivatives have been reported up to now,[26,42-45] and these are the first $[M(dppz)_3]^{n+}$ or $[M(dppn)_3]^{n+}$ complexes to be characterised in this way. Both compounds are low spin, as expected for iron(II) complexes of this type,[24] and each contains two unique complex molecules in its asymmetric unit (ESI†). The unique molecules in both structures have essentially identical metal coordination spheres, but differ in the degree of bending or twisting of their annelated ligands. The structures show substantial interdigitation between the molecules, to form 3D arrays of intermolecularly π-stacked ligands. In **4** this network is formed from π-π tetrads in the (001) plane, which are linked into 3D by an additional π-π interaction to form a closed lattice with no solvent-accessible space (ESI†).[46] In contrast, the packing in **5**·3MeOH·H_2O comprises infinite chains of π-stacked molecules parallel to [100], which are also linked by an additional pairwise interaction. This motif affords two types of rectangular channel parallel to [100], whose contents were modelled with partial methanol and water sites (Fig. 5 and ESI†). While the solvent in the smaller channels (4.2 x 4.8 Å) is well defined, the larger channels (8.3 x 8.8 Å) contain significant unresolved electron density. The solvent content in the formula of the crystal was assigned from a *SQUEEZE* analysis.[46]

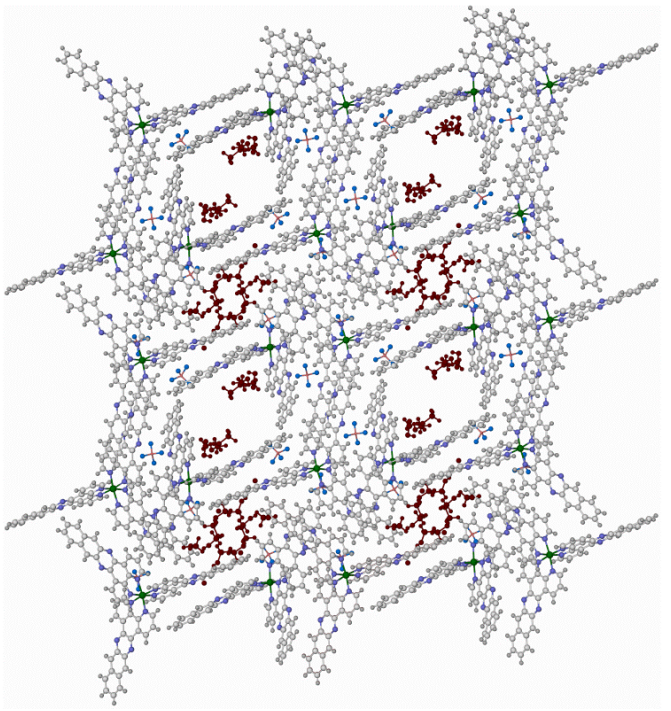

Figure 5 Packing diagram of **5**·3MeOH·H_2O, showing the large and small channels of solvent. The view is parallel to the crystallographic [100] vector, with the *b* axis vertical. Colour code; C, white; H, pale gray; B, pink; F, cyan; Fe, green; N, blue; resolved partial MeOH and H_2O solvent sites, dark red.

Conclusion

This crystallographic study has shed new light on members of the $[Fe(NCS)_2L_2]$ family (*L* = a bipyridyl derivative; Scheme 1), which have been some of the most important compounds in SCO research for the last 50 years.[47] We were originally inspired to extend the well-known structure:function relationship in these compounds, where increased conjugation of the *L* ligand leads to more cooperative and hysteretic SCO.[16] However, unexpectedly, solvent-free forms of **1**-**3** proved to be low-spin and inactive towards SCO at room-temperature or below. Crystal structure determinations of **1** and **2** demonstrate that this may reflect their crystal packing, which is based on 1D chains of molecules with interdigitated *L* ligands. However, without solvent molecules to act as a spacer (Fig. 3), the packing of the molecular chains in **1** and **2** leads to a constricted intermolecular environment, particularly about the NCS^- ligands. This includes notably short anion…π interactions between the chains, which are oriented to inhibit the expansion of the Fe–NCS units that would accompany SCO (Fig. 3). Solvent-free **3** is also isostructural with **1** and **2** by powder diffraction (ESI†).

Bulk samples of **1**-**3** are mixtures of phases, or of crystalline and amorphous material, which is particularly pronounced for **1**. Two other solvates of **1** were isolated from such mixtures by a Pasteur separation and crystallographically characterised. One of them, **1**·2py, undergoes a gradual SCO equilibrium centred at $T_{½}$ = 188±2 K, which contrasts with the abrupt and hysteretic spin transition in the corresponding solvate of **2**, **2**·py. That may reflect the much smaller change in molecular structure between the spin states in **1**·2py, which would lead to reduced intermolecular cooperativity in that material.[15] Another, possibly hydrated phase of **1** that exhibits more cooperative SCO was also evident in bulk samples, but was not obtained in single crystal form.[33]

Finally, the first crystal structures of homoleptic complexes of dppz and dppn have also been obtained. While the coordination chemistry of $[Fe(dppz)_3]^{2+}$ and $[Fe(dppn)_3]^{2+}$ is unexceptional, such three-fold symmetric complexes with extended aromatic arms could be attractive synthons for crystal engineering.[45]

Experimental

The ligands dpq,[48] dppz[49] and dppn[50] were prepared by the literature procedures. Other reagents and solvents were purchased commercially and used as supplied.

A solution of $Fe[NCS]_2$ was prepared by mixing $Fe[ClO_4]_2{\cdot}6H_2O$ (0.022 g, 0.06 mmol) with KNCS (0.012 g, 0.12 mmol) in methanol (3 cm^3), and removing the $KClO_4$ precipitate by filtration. The filtrate was layered on top of a solution of a solution of the appropriate *L* ligand (0.05 g) in 1,2-dichloroethane (5 cm^3), with a buffer layer of pure

methanol (3 cm^3) between the reagent solutions. This procedure typically yielded mixtures of powder and crystalline material, from which single crystals of **1**, **1**·2$C_2H_4Cl_2$, **2** and **4** were obtained by Pasteur separation. Crystals of **5** were prepared by the same method, using $Fe[BF_4]_2·6H_2O$ as the iron source. Slow diffusion of diethyl ether into a pyridine solution of **1** yielded a mixture of **1**·2py (plates) and $[Fe(NCS)_2(py)_2(dpq)]·py$ (needles), which was identified from the initial solution of a twinned dataset.[41]

Single crystal X-ray structure determinations

Diffraction data from **4** were measured with synchrotron radiation at station I19 of the Diamond Light Source (λ = 0.6889 Å), employing a Rigaku Saturn diffractometer. All the other crystallographic data were measured with an Agilent Supernova dual-source diffractometer, using monochromated Mo-K_α (λ = 0.7107 Å) or Cu-K_α (λ = 1.5418 Å) radiation. Both diffractometers were fitted with Oxford Cryostream low-temperature devices. Experimental details of the structure determination are given in Table 3. The structures were all solved by direct methods (*SHELXS97*[51]), and developed by full least-squares refinement on F^2 (*SHELXL97*[51]). Crystallographic figures were prepared using *XSEED*,[52] and coordination volumes (V_{Oh}, Table 1) were calculated using *Olex2*.[53]

The same crystal was used for data collections of the same compound at multiple temperatures except for **1**·2py. One crystal of that compound was used at 120 and 290 K and another for the intermediate temperatures, which were measured at a later date after the original crystal had decomposed.

Table 3 Experimental details for the crystal structure determinations in this work.

	1·2$C_2H_4Cl_2$	**1**·2py				
T (K)	100(2)	120(2)	160(2)	200(2)	240(2)	290(2)
Molecular formula	$C_{34}H_{24}Cl_4FeN_{10}S_2$	$C_{40}H_{26}FeN_{12}S_2$	$C_{40}H_{26}FeN_{12}S_2$	$C_{40}H_{26}FeN_{12}S_2$	$C_{40}H_{26}FeN_{12}S_2$	$C_{40}H_{26}FeN_{12}S_2$
M_r	834.40	794.70	794.70	794.70	794.70	794.70
Crystal class	triclinic	monoclinic	monoclinic	monoclinic	monoclinic	monoclinic
Space group	$P\bar{1}$	$P2_1/n$	$P2_1/n$	$P2_1/n$	$P2_1/n$	$P2_1/n$
a (Å)	8.6431(3)	13.3290(9)	13.3521(4)	13.4396(3)	13.4781(9)	13.5260(6)
b (Å)	12.5380(5)	16.1844(9)	16.1985(5)	16.2494(3)	16.2943(12)	16.3143(6)
c (Å)	16.8933(7)	17.3536(8)	17.4429(4)	17.5932(4)	17.6998(12)	17.8163(8)
α (°)	100.234(3)	–	–	–	–	–
β (°)	97.965(3)	110.324(7)	110.287(3)	110.306(2)	110.310(8)	110.291(5)
γ (°)	101.090(3)	–	–	–	–	–
V ($Å^3$)	1739.40(12)	3510.5(3)	3538.59(17)	3603.32(13)	3645.5(4)	3687.5(3)
Z	2	4	4	4	4	4
μ (mm^{-1})	7.785[a]	4.971[a]	4.932[a]	4.843[a]	4.787[a]	4.733[a]
Measured reflections	12817	14631	16044	15490	16575	18017
Independent reflections	6537	6905	6708	6836	6870	7093
R_{int}	0.026	0.030	0.043	0.039	0.059	0.031
R_1, $I > 2\sigma(I)$[d]	0.042	0.038	0.051	0.049	0.059	0.046
wR_2, all data[e]	0.113	0.095	0.145	0.139	0.186	0.128
	1		**2**		**4**	**5**·3MeOH·H_2O
T (K)	120(2)	290(2)	120(2)	290(2)	173(2)	120(2)
Molecular formula	$C_{30}H_{16}FeN_{10}S_2$	$C_{30}H_{16}FeN_{10}S_2$	$C_{38}H_{20}FeN_{10}S_2$	$C_{38}H_{20}FeN_{10}S_2$	$C_{54}H_{30}Cl_2FeN_{12}O_8$	$C_{69}H_{50}B_2F_8FeN_{12}O_4$
M_r	636.50	636.50	736.61	736.61	1101.65	1340.68
Crystal class	monoclinic	monoclinic	monoclinic	monoclinic	monoclinic	triclinic
Space group	*C*2/*c*	*C*2/*c*	*C*2/*c*	*C*2/*c*	$P2_1/c$	$P\bar{1}$
a (Å)	7.7346(7)	7.7581(14)	7.9867(4)	8.0689(4)	24.6343(9)	9.7973(2)
b (Å)	14.8899(13)	15.139(3)	14.6323(6)	14.7987(6)	21.2193(4)	23.8139(8)
c (Å)	23.801(2)	23.695(6)	28.1005(15)	28.0208(12)	18.1944(5)	27.5891(6)
α (°)	–	–	–	–	–	95.037(2)
β (°)	94.674(9)	93.796(18)	93.360(5)	92.552(4)	104.239(3)	98.452(2)
γ (°)	–	–	–	–	–	93.612(2)
V ($Å^3$)	2731.9(4)	2776.9(10)	3278.3(3)	3342.6(3)	9218.4(5)	6323.5(3)
Z	4	4	4	4	8	4
μ (mm^{-1})	0.747[b]	0.735[b]	5.259[a]	5.158[a]	0.519[c]	2.631[a]
Measured reflections	8075	6710	5461	7733	122082	56368
Independent reflections	2967	2944	3181	3232	16170	23938
R_{int}	0.047	0.040	0.047	0.046	0.167	0.069
R_1, $I > 2\sigma(I)$[d]	0.053	0.061	0.060	0.059	0.064	0.085
wR_2, all data[e]	0.109	0.122	0.160	0.164	0.182	0.269

[a]Collected with Cu-*Kα* radiation. [b]Collected with Mo-*Kα* radiation. [c]Collected with synchrotron radiation. [d]$R = \Sigma[|F_o| - |F_c|] / \Sigma|F_o|$. [e]$wR = [\Sigma w(F_o^2 - F_c^2) / \Sigma wF_o^4]^{1/2}$

X-ray structure refinements

Unless otherwise stated, all non-H atoms in the structures were refined anisotropically, while H atoms were placed in calculated positions and refined using a riding model.

The solvent-free crystals of **1** and **2** are isostructural. Their asymmetric units contain half a molecule, with Fe(1) lying on a crystallographic C_2 axis. The C and S atoms of the unique NCS^- ligand in **1**, and in **2** at 290 K, are disordered over two orientations which were modelled without restraints. In each case, the occupancies of the disorder sites refined to 0.60:0.40±0.02. The NCS^- ligand in **2** at 120 K is crystallographically ordered. All non-H atoms were refined anisotropically except, where applicable, the minor ligand disorder site.

The asymmetric unit of **1**·2py contains one molecule of the complex and two molecules of pyridine, all on general crystallographic sites. One of the pyridine molecules is disordered over two sites at all five temperatures, which were modelled without restraints. The occupancy ratio of these partial solvent sites refined within the range 0.59:0.41 – 0.67:0.33 at the different temperatures. All non-H atoms were refined anisotropically except, where appropriate, the disordered solvent molecule. The asymmetric unit of **1**·$2C_2H_4Cl_2$ contains one molecule of the complex, one whole molecule of 1,2-dichloroethane and two half-molecules of the same solvent spanning crystallographic inversion centres. The methylene group of one of these solvent half-molecules is disordered over two sites, with refined occupancies of 0.62:0.38. These were modelled without restraints.

The asymmetric unit of **4** contains two formula units (*i.e. Z*′ = 2), with two complex cations and four anions lying on general crystallographic positions. One anion was clearly disordered and modelled over three orientations, with a 0.5:0.25:0.25 occupancy ratio. The fixed restraints Cl–O = 1.45(2) and O...O = 2.37(2) Å were applied to this residue. All non-H atoms except the disordered anion were refined anisotropically.

The asymmetric unit of **5**·3MeOH·H_2O also contains two formula units of the compound (*Z*′ = 2). That is, two complex dications, four BF_4^- ions and a number of part occupied, disordered solvent molecules that were modelled as a mixture of methanol and water. The solvent occupied two different types of channel, which both run parallel to the crystallographic *a* axis. A *SQUEEZE* analysis[46] from a model containing only the cations and anions showed 1337 $Å^3$ of void space, which is 21 % of the unit cell volume. The voids were occupied by 249 unresolved electrons per unit cell, or 62.25 per formula unit. That is close to a solvent complement of 3x methanol (3x 18 electrons) and 1x water (10 electrons), which would equate to 64 electrons in total. That formula was used for the density and *F*(000) calculations in the cif file. For comparison, the final refinement model contains solvent sites summing to 1.5 equiv of methanol and 0.85 equiv water, per formula unit. The original dataset, rather than the *SQUEEZE*d one, was used in the final refinement cycles. The partial methanol C–O bonds were restrained to 1.43(2) Å, but no other restraints were applied. All wholly occupied non-H atoms were refined anisotropically. The partial water H atoms were not located in Fourier map, and are not included in the model.

Acknowledgements

The authors thank Dr Oscar Cespedes (School of Physics and Astronomy, University of Leeds) for help with the magnetic susceptibilty measurements. We also thank Diamond Light Source for access to beamline I19 (MT10334) that contributed to the results presented here. This work was funded by EPSRC grants EP/K012568/1 and EP/K00512X/1.

Notes and references

1 P. Gutlich and H. A. Goodwin (Eds.), *Spin-Crossover in Transition-Metal Compounds I–III, in: Topics in Current Chemistry*, vol. **233–235**, Springer, Berlin, 2004.

2 M. A. Halcrow (Ed.), *Spin-crossover Materials – Properties and Applications*, John Wiley & Sons, Chichester, UK, 2013, p. 568.

3 A. Bousseksou, G. Molnár, L. Salmon and W. Nicolazzi, *Chem. Soc. Rev.*, 2011, **40**, 3313; P. Gütlich, *Eur. J. Inorg. Chem.*, 2013, 581.

4 O. Kahn, J. Kröber and C. Jay, *Adv. Mater.*, 1992, **4**, 718.

5 M. Matsuda and H. Tajima, *Chem. Lett.*, 2007, **36**, 700; W. Xue, B.-Y. Wang, J. Zhu, W.-X. Zhang, Y.-B. Zhang, H.-X. Zhao and X.-M. Chen, *Chem. Commun.*, 2011, **47**, 10233; A. Rotaru, I. A. Gural'skiy, G. Molnár, L. Salmon, P. Demont and A. Bousseksou, *Chem. Commun.*, 2012, **48**, 4163.

6 M. Nakano, G. Matsubayashi and T. Matsuo, *Phys. Rev. B*, 2002, **66**, 21241/1; A. Bousseksou, G. Molnár, P. Demont and J. Menegotto, *J. Mater. Chem.*, 2003, **13**, 2069; S. Bonhommeau, T. Guillon, L. M. L. Daku, P. Demont, J. S. Costa, J.-F. Létard, G. Molnár and A. Bousseksou, *Angew. Chem., Int. Ed.*, 2006, **45**, 1625; X. Zhang, S. Mu, G. Chastanet, N. Daro, T. Palamarciuc, P. Rosa, J.-F. Létard, J. Liu, G. E. Sterbinsky, D. A. Arena, C. Etrillard, B. Kundys, B. Doudin and P. A. Dowben, *J. Phys. Chem. C*, 2015, **119**, 16293.

7 M. D. Manrique-Juárez, S. Rat, L. Salmon, G. Molnár, C. M. Quintero, L. Nicu, H. J. Shepherd and A. Bousseksou, *Coord. Chem. Rev.*, 2016, **308**, 395.

8 A. B. Gaspar, V. Ksenofontov, M. Seredyuk and P. Gütlich, *Coord. Chem. Rev.*, 2005, **249**, 2661.

9 See *eg* Y. Garcia, F. Robert, A. D. Naik, G. Zhou, B. Tinant, K. Robeyns, S. Michotte and L. Piraux, *J. Am. Chem. Soc.*, 2011, **133**, 15850; C.-F. Wang, R.-F. Li, X.-Y. Chen, R.-J. Wei, L.-S. Zheng and J. Tao, *Angew. Chem., Int. Ed.*, 2015, **54**, 1574; J. M. Herrera, S. Titos-Padilla, S. J. A. Pope, I. Berlanga, F. Zamora, J. J. Delgado, K. V. Kamenev, X. Wang, A. Prescimone, E. K. Brechin and E. Colacio, *J. Mater. Chem. C*, 2015, **3**, 7819.

10 See *eg* K. Takahashi, H.-B. Cui, Y. Okano, H. Kobayashi, H. Mori, H. Tajima, Y. Einaga and O. Sato, *J. Am. Chem. Soc.*, 2008, **130**, 6688; M. Nihei, N. Takahashi, H. Nishikawa and H. Oshio, *Dalton Trans.*, 2011, **40**, 2154; H. Phan, S. M. Benjamin, E. Steven, J. S. Brooks and M. Shatruk, *Angew. Chem., Int. Ed.*, 2015, **54**, 823.

11 See eg S. Ohkoshi, K. Imoto, Y. Tsunobuchi, S. Takano and H. Tokoro, *Nature Chem.*, 2011, **3**, 564; J. H. Yoon, D. W. Ryu, S. Y. Choi, H. C. Kim, E. K. Koh, J. Tao and C. S. Hong, *Chem. Commun.*, 2011, **47**, 10416; R. Ababei, C. Pichon, O. Roubeau, Y.-G. Li, N. Bréfuel, L. Buisson, P. Guionneau, C.

Mathonière and R. Clérac, *J. Am. Chem. Soc.*, 2013, **135**, 14840.
12 A. B. Gaspar and M. Seredyuk, *Coord. Chem. Rev.*, 2014, **268**, 41.
13 M. Cavallini, *Phys. Chem. Chem. Phys.*, 2012, **14**, 11867; H. J. Shepherd, G. Molnár, W. Nicolazzi, L. Salmon and A. Bousseksou, *Eur. J. Inorg. Chem.*, 2013, 653.
14 M. Mikolasek, G. Félix, W. Nicolazzi, G. Molnár, L. Salmon and A. Bousseksou, *New J. Chem.*, 2014, **38**, 1834.
15 M. A. Halcrow, *Chem. Soc. Rev.*, 2011, **40**, 4119.
16 J. A. Real, A. B. Gaspar, V. Niel and M. C. Muñoz, *Coord. Chem. Rev.*, 2003, **236**, 121.
17 G. Bradley, V. McKee, S. M. Nelson and J. Nelson, *J. Chem. Soc., Dalton Trans.*, 1978, 522; J. A. Real, B. Gallois, T. Granier, F. Suez-Panama and J. Zarembowitch, *Inorg. Chem.*, 1992, **31**, 4972.
18 E. König, K. Madeja and K. J. Watson, *J. Am. Chem. Soc.*, 1968, **90**, 1146; M. Konno and M. Mikami-Kido, *Bull. Chem. Soc. Jpn.*, 1991, **46**, 339.
19 E. König and K. Madeja, *Inorg. Chem.*, 1967, 6, 48; B. Gallois, J. A. Real, C. Hauw and J. Zarembowitch, *Inorg. Chem.*, 1990, **29**, 1152.
20 Z. J. Zhong, J.-Q. Tao, Z. Yu, C.-Y. Dun, Y.-J. Liu and X.-Z. You, *J. Chem. Soc., Dalton Trans.*, 1998, 327. The space-group of $[Fe(NCS)_2(dppz)_2]\cdot py$ (**2**·py) is mis-assigned in this paper.[21]
21 J. Kusz, M. Zubko, A. Fitch and P. Gütlich, *Z. Kristallogr.*, 2011, **226**, 576.
22 H. J. Shepherd, T. Palamarciuc, P. Rosa, P. Guionneau, G. Molnár, J.-F. Létard and A. Bousseksou, *Angew. Chem., Int. Ed.*, 2012, **51**, 3910.
23 N. Paradis, G. Chastanet, T. Palamarciuc, P. Rosa, F. Varret, K. Boukheddaden and J.-F. Létard, *J. Phys. Chem. C*, 2015, **119**, 20039.
24 Other compounds from the $[Fe(NCS)_2L_2]$ and $[FeL_3]^{2+}$ families are tabulated in M. A. Halcrow, *Polyhedron*, 2007, **26**, 3523.
25 P. Guionneau, M. Marchivie, G. Bravic, J.-F. Létard and D. Chasseau, *Top. Curr. Chem.*, 2004, **234**, 97 and refs therein.
26 Y. Shuku, R. Suizu, K. Awaga and O. Sato, *CrystEngComm*, 2009, **11**, 2065.
27 Q. Yang, X. Cheng, Y. X. Wang, B. W. Wang, Z. M. Wang and S. Gao, *Dalton Trans.*, 2015, **44**, 8938; Q. Yang, X. Cheng, C. Gao, B. W. Wang, Z. M. Wang and S. Gao, *Cryst. Growth Des.*, 2015, **15**, 2565.
28 M. Quesada, M. Monrabal, G. Aromí, V. A. de la Peña-O'Shea, M. Gich, E. Molins, O. Roubeau, S. J. Teat, E. J. MacLean, P. Gamez and J. Reedijk, *J. Mater. Chem.*, 2006, **16**, 2669; N. Wannarit, O. Roubeau, S. Youngme, S. J. Teat and P. Gamez, *Dalton Trans.*, 2013, **42**, 7120; N. Wannarit, O. Roubeau, S. Youngme and P. Gamez, *Eur. J. Inorg. Chem.*, 2013, 730; N. Nassirinia, S. Amani, S. J. Teat, O. Roubeau and P. Gamez, *Chem. Commun.*, 2014, **50**, 1003; H. S. Scott, T. M. Ross, W. Phonsri, B. Moubaraki, G. Chastanet, J.-F. Létard, S. R. Batten and K. S. Murray, *Eur. J. Inorg. Chem.*, 2015, 763; H. S. Scott, B. Moubaraki, N. Paradis, G. Chastanet, J.-F. Létard, S. R. Batten and K. S. Murray, *J. Mater. Chem. C*, 2015, **3**, 7845.
29 Another well-known family of $[Fe(NCS)_2L_2]$ SCO complexes, where *L* is a ligand derived from 2,5-di(pyrid-2-yl)-1,3,4-triazole, usually exhibit trans NCS^- ligands. J. A. Kitchen and S. Brooker, *Coord. Chem. Rev.*, 2008, **252**, 2072.
30 R. Kulmaczewski, H. J. Shepherd, O. Cespedes and M. A. Halcrow, *Inorg. Chem.*, 2014, **53**, 9809.
31 A. Santoro, L. J. Kershaw Cook, R. Kulmaczewski, S. A. Barrett, O. Cespedes and M. A. Halcrow, *Inorg. Chem.*, 2015, **54**, 682.
32 H. van der Salm, A. B. S. Elliott and K. C. Gordon, *Coord. Chem. Rev.*, 2015, **282–283**, 33.
33 Compound **1** has been described before in the Chinese literature, where a hydrated material $\mathbf{1}\cdot{}^3/_2H_2O$ was reported to undergo SCO with a 15 K hysteresis loop. J.-Q. Tao, W.-Z. Shi, X. Zhuang, Z. Yu and X.-Z. You, *Wuji Huaxue Xuebao*, 2002, **18**, 255.
34 R. Claude, J. A. Real, J. Zarembowitch, O. Kahn, L. Ouahab, D. Grandjean, K. Boukheddaden, F. Varret and A. Dworkin, *Inorg. Chem.*, 1990, **29**, 4442; J.-Q. Tao, Z.-G. Gu, T.-W. Wang, Q.-F. Yang, J.-L. Zuo and X.-Z. You, *Inorg. Chim. Acta*, 2007, **360**, 4125; J. Tao, Y. Gu, X. Zhou, Z. Gu, J. Zuo and X. You, *Chin. J. Chem.*, 2009, **27**, 1280.
35 Σ is a general measure of the deviation of a metal ion from an ideal octahedral geometry, while Θ more specifically indicates its distortion towards a trigonal prismatic structure.[25,36,37] Both Σ and Θ are usually larger in the high-spin than in the low-spin state; a perfectly octahedral complex gives $\Sigma = \Theta = 0$. Mathematical definitions of Σ and Θ are in ref. 25, and the ESI†.
36 J. K. McCusker, A. L. Rheingold and D. N. Hendrickson, *Inorg. Chem.*, 1996, **35**, 2100–2112.
37 M. Marchivie, P. Guionneau, J.-F. Létard and D. Chasseau, *Acta Cryst., Sect. B*, 2005, **61**, 25–28.
38 In view of the magnetic susceptibility data from **1**-**3**, which sometimes indicated the onset of gradual SCO above room temperature (ESI†), a crystal structure of **2** at 350 K was also attempted. While the crystal had the same space group and comparable unit cell parameters as at lower temperatures, its mosaicity had increased and it diffracted too weakly at 350 K to permit a full refinement. Unit cell parameters of **2** at 350 K: a = 8.0710(16), b = 14.961(2), c = 28.003(6) Å, β = 91.56(2)°, V = 3380.0(11) Å^3.
39 D. Onggo, A. D. Rae and H. A. Goodwin, *Inorg. Chim. Acta*, 1990, **178**, 151.
40 A. Frontera, P. Gamez, M. Mascal, T. J. Mooibroek and J. Reedijk, *Angew. Chem., Int. Ed.*, 2011, **50**, 9564; H. T. Chifotides and K. R. Dunbar, *Acc. Chem. Res.*, 2013, **46**, 894.
41 Unit cell parameters of $[Fe(NCS)_2(py)_2(dpq)]\cdot py$ at 120 K: $C_{31}H_{24}FeN_9S_2$, M_r = 642.57, monoclinic, $P2/n$, a = 12.4914(11), b = 13.6836(9), c = 17.1800(12) Å, β = 104.523(8)°, V = 3380.0(11) Å^3. The asymmetric unit of the twinned crystal contains two half-molecules of the complex, each with crystallographic C_2 symmetry, and a whole molecule of pyridine on a general position (ESI†).
42 B. de Souza, F. R. Xavier, R. A. Peralta, A. J. Bortoluzzi, G. Conte, H. Gallardo, F. L. Fischer G. Bussi, H. Terenzi and A. Neves, *Chem. Commun.*, 2010, **46**, 3375.
43 M. Roy, B. Pathak, A. K. Patra, E. D. Jemmis, M. Nethaji and A. R. Chakravarty, *Inorg. Chem.*, 2007, **46**, 11122.
44 A. Chouai, S. E. Wicke, C. Turro, J. Bacsa, K. R. Dunbar, D. Wang and R. P. Thummel, *Inorg. Chem.*, 2005, **44**, 5996.
45 S. Kammer, H. Müller, N. Grunwald, A. Bellin, A. Kelling, U. Schilde, W. Mickler, C. Dosche and H.-J. Holdt, *Eur. J. Inorg. Chem.*, 2006, 1547.
46 A. L. Spek, *J. Appl. Cryst.*, 2003, **36**, 7.
47 M. A. Halcrow, *Chem. Commun.*, 2013, **49**, 10890.
48 J. G. Collins, A. D. Sleeman, J. R. Aldrich-Wright, I. Greguric, and T. W. Hambley, *Inorg. Chem.*, 1998, **37**, 3133.
49 C. M. Dupureur and J. K. Barton, *Inorg. Chem.*, 1997, **36**, 33.
50 A. J. McConnell, M. H. Lim, E. D. Olmon, H. Song, E. E. Dervan and J. K. Barton, *Inorg. Chem.*, 2012, **51**, 12511.
51 G. M. Sheldrick, *Acta Cryst., Sect. A*, 2008, **64**, 112.
52 L. J. Barbour, *J. Supramol. Chem.*, 2001, **1**, 189.
53 O. V. Dolomanov, L. J. Bourhis, R. J. Gildea, J. A. K. Howard and H. Puschmann, *J. Appl. Cryst.*, 2009, **42**, 339.